Geochemistry Geophysics Geosystems G3
AN ELECTRONIC JOURNAL OF THE EARTH SCIENCES
Published by AGU and the Geochemical Society

Article
Volume 6, Number 1
27 January 2005
Q01H14, doi:10.1029/2004GC000839
ISSN: 1525-2027

On the use of magnetic transient hysteresis in paleomagnetism for granulometry

Yongjae Yu and Lisa Tauxe
Scripps Institution of Oceanography, La Jolla, California 92093-0220, USA (yjyu@ucsd.edu)

[1] Parameters derived from magnetic hysteresis experiments have been used as granulometric indicators in paleomagnetism. In practice, discriminating the superparamagnetic (SP) fraction from the coarse grain magnetites in parameter ratio plots is often inconclusive. To overcome this ambiguity, transient hysteresis (TH) has been recently proposed. We have carried out micromagnetic simulations to provide a fundamental rationale for the use of TH for granulometry. We found that magnetic TH results from the difference of magnetization configuration between ascending and descending hysteresis loops as a result of self-demagnetization. The descending branch has a tendency to keep a more uniform (e.g., flower-like) configuration, while the ascending branch prefers a less uniform (e.g., vortex-like) structure. According to our simulations, TH increases as the grain size increases and as the aspect ratio decreases. We also carried out TH measurements for well-defined synthetic and natural samples. It is notable that TH from the simulation for samples with aspect ratio q = 1.5 agrees well with the experimental observations for annealed magnetites of smaller sizes. In general, small TH is a clear indication for the absence of complex magnetized structures. Adding TH analysis to the hysteresis loop measurements requires a minor effort yet provides strong constraint on grain size.

Components: 5953 words, 14 figures, 2 tables.

Keywords: FORC; granulometry; hysteresis; magnetite; transient hysteresis.

Index Terms: 1540 Geomagnetism and Paleomagnetism: Rock and mineral magnetism; 1594 Geomagnetism and Paleomagnetism: Instruments and techniques; 1599 Geomagnetism and Paleomagnetism: General or miscellaneous.

Received 8 September 2004; **Revised** 5 November 2004; **Accepted** 1 December 2004; **Published** 27 January 2005.

Yu, Y., and L. Tauxe (2005), On the use of magnetic transient hysteresis in paleomagnetism for granulometry, *Geochem. Geophys. Geosyst.*, *6*, Q01H14, doi:10.1029/2004GC000839.

Theme: Geomagnetic Field Behavior Over the Past 5 Myr
Guest Editors: Cathy Constable and Catherine Johnson

1. Introduction

[2] In environmental, paleo-, and rock magnetism, measuring magnetic hysteresis has become a routine process for characterizing the magnetic properties of rocks. In general, values of M_s (saturation magnetization), M_r (saturation remanence), and B_c (coercivity) are determined from hysteresis loops after an appropriate nonferrimagnetic slope correction (Figure 1a). Values of B_c and the ratio M_r/M_s (=hereafter squareness) provide the most convenient (yet complicated) quantities to estimate domain state of the magnetic phases in the rocks. Despite their common use, hysteresis properties often provide inconclusive information on average grain size of magnetic minerals because hysteresis behavior is governed by many factors, such as composition, initial state, grain-shape and size, stress, and temperature.

[3] Recently, *Fabian* [2003] proposed a new rock magnetic parameter derived from hysteresis experi-

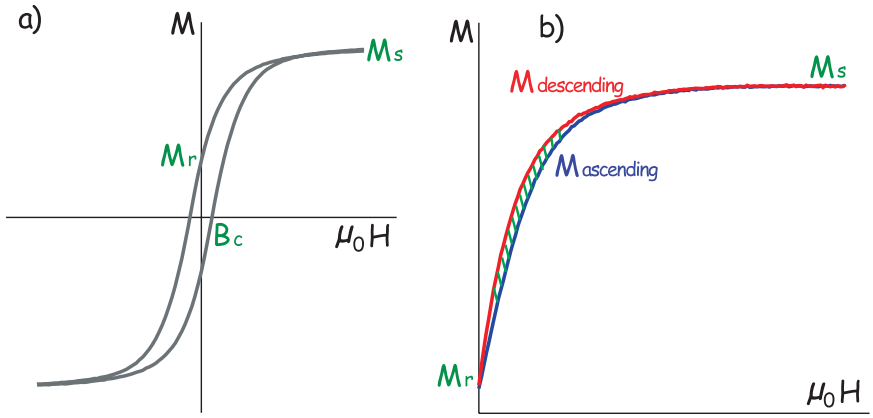

Figure 1. (a) A typical magnetic hysteresis loop. Definitions of M_s, M_r, and B_c are shown. (b) Measuring magnetic transient hysteresis (TH), which is the area between the descending and ascending loops (shaded area).

ments: transient hysteresis (TH). In empirical form, TH is the summation of the difference between the ascending and descending branches of partial hysteresis experiment that cycles from saturation to remanence state, and then back to saturation magnetization state (Figure 1b). This is one of a special form of hysteresis experiments known as "first-order reversing curves," or FORCs [*Mayergoyz*, 1986], in which the turning point is at zero field. In the present study, these special FORCs are denoted as zero-FORC or ZFORC. TH is defined as

$$TH = \sum_{\mu_0 H=0}^{\mu_0 H_{\max}} \left[M_{descending} - M_{ascending} \right] \cdot \Delta H, \qquad (1)$$

where ΔH is a fixed field-increment (e.g., 1 mT) used in hysteresis measurements. If we normalize magnetization to M_s, TH has a units of induction field (e.g., mT).

[4] Because the difference between the ascending and descending branches results from the action of self-demagnetization, TH represents the degree of irreversible hysteresis behavior [*Fabian*, 2003]. In other words, TH is absent in superparamagnetic (SP) or ideal single-domain (SD) grains whose remanent states are uniform or nearly uniform. Large particles with complex magnetic remanent states or those that contain domain walls exhibit transient hysteresis because the formation of these patterns of magnetization occurs at different fields on the descending branch than their destruction on the ascending branch.

[5] Micromagnetism concerns the calculation of detailed magnetization configurations and the magnetic reversal process in a magnetic system. Not only can micromagnetic calculations predict complex magnetic domain structures, they can also produce transient pictures of complex domain configurations [e.g., *Schabes and Bertram*, 1988]. The general method of micromagnetism involves considering all the fundamental energies at near atomic levels. The underlying assumption is that within a small element of volume, atomic spins are approximately parallel to one another, or at least a linear function of position. Unlike in classical domain theory of ferrimagnetism, micromagnetism shows that the most common remanent states are dominated by nonuniform magnetizations. Micromagnetic modeling is therefore necessary to decipher the fundamental behavior of nonuniform magnetization structures.

[6] The present study was intended (1) to elucidate fundamental aspects of TH from micromagnetic modeling, (2) to compare model predictions with the experimental observations, and (3) to provide a quick and useful granulometric indicator in paleomagnetism.

2. Micromagnetic Modeling

2.1. Some Preliminaries

[7] On the basis of micromagnetic theory with adequate descriptions of magnetization directions, we can model magnetic hysteresis. The total magnetic energy of the system is a summation of the exchange energy that keeps the adjacent spins parallel to one another, magnetocrystalline energy that preferentially orients magnetic moments near the easy axis of the grain, magnetostatic energy due to the divergence of the magnetization, magnetic potential energy resulting from the existence of an

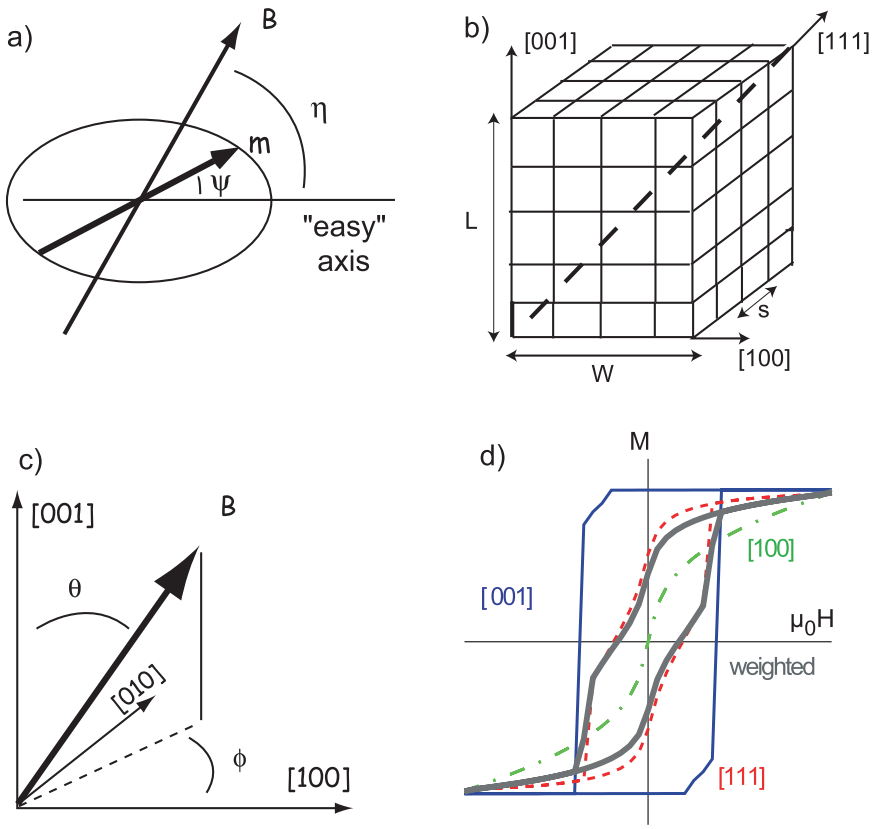

Figure 2. A reference frame for micromagnetic simulation. (a) Relationship of applied field B, easy axis of magnetic particle, and the magnetization vector M of the particle. η is the angle of the easy axis of the grain with respect to the applied field B, and ψ is the angle of the magnetization with respect to the easy axis. (b) Partition of the particle with width W, length L, and cell size s. (c) Relationship between applied field and crystallographic axis. (d) Simulation of magnetic hysteresis of 4 × 4 × 6 40 nm magnetite. Magnetic hysteresis shows strong angular dependence. We used Euler angle approximation (see section 3.2) to calculate the weighted hysteresis for randomly oriented grains.

external field, and magnetoelastic energy owing to lattice distortions of magnetic minerals. The distribution of magnetization orientations in a given configuration is found by minimizing the total free energy.

[8] For uniformly magnetized samples, magnetization in the remanence state is mostly controlled by exchange anisotropy. An analytical solution for this ideal case has long been recognized for noninteracting ideal SD grains [see *Stoner and Wohlfarth*, 1948]:

$$E_t = K_u \sin^2\psi - M_s B\cos(\eta - \psi), \tag{2}$$

where E_t is the total energy, η is the angle of the easy axis of the grain with respect to the applied field B, and ψ is the angle of the magnetization with respect to the easy axis (Figure 2a). Uniaxial anisotropy originates from the shape of the magnetic grains and the anisotropy constant is given by

$$K_u = (1/2)\mu_0(\Delta N)M_s^2, \tag{3}$$

where ΔN is a shape factor that ranges from 0 (for equant particle) to 1 (for an extremely prolate particle).

[9] For equant grains of magnetite, the anisotropy is dominated by the crystalline structure

$$E_a = K_1\left(\alpha_1^2\alpha_2^2 + \alpha_2^2\alpha_3^2 + \alpha_3^2\alpha_1^2\right) + K_2\left(\alpha_1^2\alpha_2^2\alpha_3^2\right), \tag{4}$$

where E_a is the magnetocrystalline energy, K_1 and K_2 are the constants of magnetocrystalline anisotropy, and the αs are direction cosines between magnetization and the three major crystallographic axes [001, 100, 010].

[10] Fast computer-based micromagnetic models have successfully revealed complicated magnetization structures [e.g., *Schabes and Bertram*, 1988; *Williams and Dunlop*, 1989, 1990; *Schabes*, 1991]. The most profound discovery from these simulations was the discovery of the evolution of nonuniform magnetization states from the uniform magnetization state in SD to distinct domain walls in MD. Whether it was a 2-dimensional or 3-dimensional investigation, there has been much progress in modeling of magnetic grains of paleomagnetic interests [see *Williams and Dunlop*, 1995; *Fabian et al.*, 1996; *Fukuma and Dunlop*, 1997, 1998; *Rave and Ramstock*, 1997; *Winklhofer et al.*, 1997; *Rave et al.*, 1998; *Williams and Wright*, 1998; *Muxworthy and Williams*, 1999a, 1999b; *Newell and Merrill*, 2000a, 2000b; *Tauxe et al.*, 2002; *Carvallo et al.*, 2003; *Muxworthy et al.*, 2003a, 2003b].

[11] In particular, modeling magnetic hysteresis has received special attention due to its practical importance in paleomagnetism. *Williams and Dunlop* [1995] simulated magnetic hysteresis for 0.1–0.7 μm magnetite cubes and parallelepipeds along the easy and hard axes. They concluded that a vortex remanence state is responsible for the so-called "pseudo-single-domain (PSD)" behavior of magnetic hysteresis. *Fabian et al.* [1996] studied the remanence states of magnetite grains with aspect ratios ranging from 1 to 2.74 for 0.05–0.6 μm magnetite. They determined ranges of the SD-PSD boundary on the basis of energy differentials between flower and vortex remanence states. *Muxworthy and Williams* [1999a, 1999b] incorporated temperature variations in their simulations. They investigated the behavior of magnetite near the Verwey transition and as a function of temperature. *Newell and Merrill* [2000a] pointed out the instability of numerical solutions and suggested strategies to avoid unstable outcomes. In a companion paper, *Newell and Merrill* [2000b] simulated magnetic hysteresis of cubic magnetites, expressed many difficulties of using hysteresis in magnetic granulometry. In this study, we expand on the efforts of *Tauxe et al.* [2002] by simulating the partial hysteresis experiments to determine transient hysteresis as proposed by *Fabian* [2003].

2.2. Micromagnetic Simulation

[12] During the modeling process, we discretize particles into cubic elements within which magnetization is uniform (Figure 2b) [see also *Bertram and Zhu*, 1992]. The cell dimension is s. We used a Fast Multipole Code (FMM) [see *Seberino and Bertram*, 2001] that integrates the coupled Landau-Lifshitz equation. For a given input configuration of each particle, the sequential FMM decomposes the data-space in a hierarchy of blocks and computes local neighborhoods. The first pass calculates the root accumulating the multipole coefficients at intermediate tree-nodes. When the root is reached, the second pass starts where exchanging data between blocks belonging to the neighborhoods and interaction-lists calculated at tree-construction is performed. Finally, short- and long-range interactions are accumulated and the total free energies exerted upon particles are computed. The algorithm repeats the above steps and simulates the evolution of the system for each successive time step. This technique reduces the computational cost of calculating the magnetostatic field and scales asymptotically linearly with the problem size. All calculations were obtained using four PCs that are four-node partitioned. A total of >30,000 hours were consumed to complete the computations.

[13] Our numerical model considers magnetocrystalline anisotropy and attempts to incorporate the effect of size, shape, and orientation with the external field. We have neglected the effect of magnetostriction and thermal fluctuation for simplicity. In the following, we will describe our modeling procedure of magnetite particles that range from 40 to 200 nm.

[14] For each grain size, at least ten different aspect ratios from 1:1 to 2:1 were assigned. For example, for a 200 nm width grain, the aspect ratios were 1.0, 1.1, 1.2, 1.3, 1.4, 1.5, 1.6, 1.7, 1.8, 1.9, and 2.0. Keep the same element size is ideal to minimize errors for exchange anisotropy. However, this will allow only a limited number of axial ratio configuration for smaller grains. For grains <100 nm, we allowed a slight variation of element size (so does the exchange length) for each grain (e.g., 9–11 nm) to simulate various aspect ratios. On the other hand, a uniform element size (exchange length of 10 nm) was used for grains larger than 100 nm. We set elongation along the [001] direction for convenience (Figure 2b). Note that elongation along [100] or [010] yields an identical solution due to an existing cylindrical symmetry (Figure 2c). In each case, magnetic hysteresis was simulated along three different crystallographic axes [001, 100, 111] of magnetite cubes (Figures 2b and 2c). The relationship of the applied field with respect to the crystallographic axes are illustrated as θ and ϕ (Figure 2c).

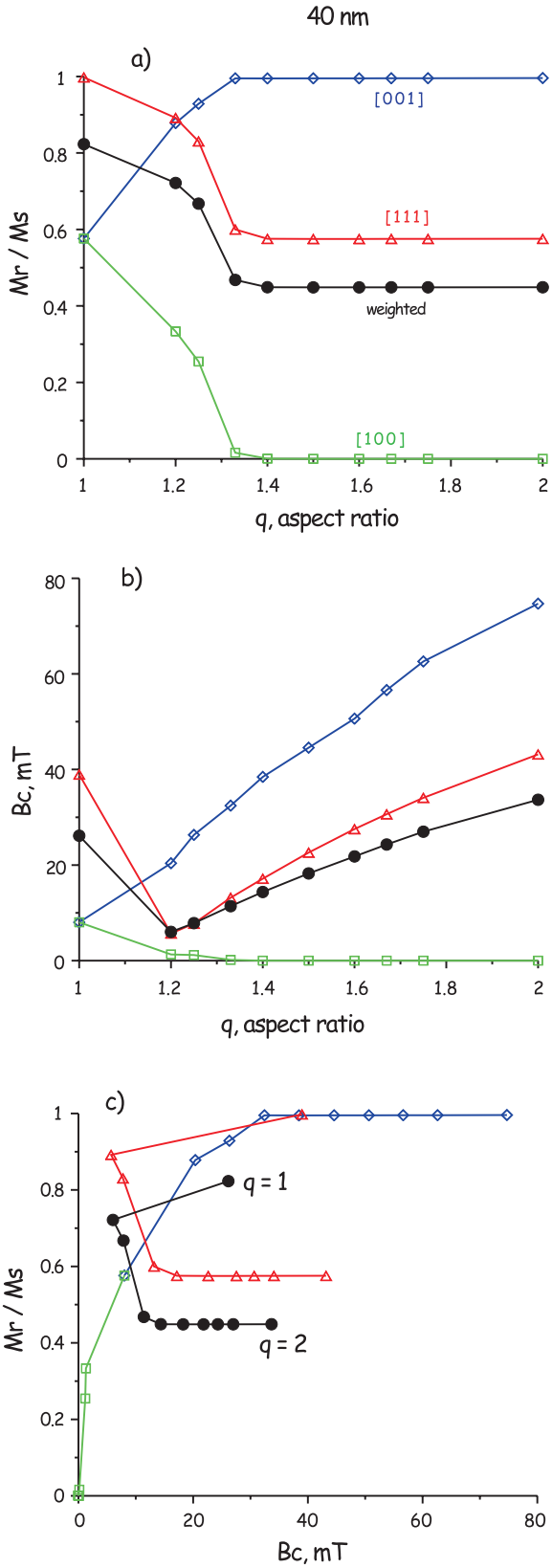

[15] For each configuration, we simulated one full hysteresis loop and the TH. To simulate TH, we have started with the magnetization that is parallel to the applied field, then applied a saturation magnetic field of 0.6 T. After saturation, we decrease the field in decrements of 6 mT to zero and evaluate squareness. We then increase the field to 0.6 T to complete the modeling of TH. To obtain a full hysteresis curve, simulations were cycled through from positive to negative saturation, then back to positive saturation magnetization state.

[16] In order to eliminate possible instability of our numerical solutions, we repeated all the simulation with different field increment/decrements of 1, 2, and 3 mT [*Newell and Merrill*, 2000b; A. Newell, personal communication]. Whenever we found dual solutions, we use the smoother (with less drastic jumps) hysteresis as the ultimate solution. The material constants, chosen for room temperature T = 298 K, were $A = 1.32 \times 10^{-11}$ J/m, $M_s = 4.80 \times 10^5$ A/m, and $K_1 = -1.25 \times 10^4$ J/m^3 [see *Tauxe et al.*, 2002].

2.3. Angular Dependence of Magnetic Hysteresis

[17] For an elongated single magnetite grain, magnetic hysteresis has a strong angular dependence. For 40 nm magnetite with 4 × 4 × 6 configuration, square-type magnetic hysteresis is produced along the elongation axis [001] but virtually no hysteresis is observed along [100]. Hysteresis along [111] falls between them (Figure 2d).

[18] In practice, we are dealing with an assemblage of uniaxial (or cubic) grains that have random orientations of their easy axes. How can we determine the hysteresis produced by a set of randomly oriented grains? Although carrying out many simulations along random orientations or mathematically calculating integrated hysteresis over all possible angles would be an ultimate solution [*Tauxe et al.*, 1996, 2002], we found that Euler angle approximation [see *Arfken and Weber*, 1995,

Figure 3. Hysteresis parameters for 40 nm grains of magnetite along different axes. Diamonds are along [001], squares are along [100], and triangles are along [111]. The weighted averages (approximation of random assemblages) are displayed as solid circles. Variation of (a) squareness (=M_r/M_s) and (b) coercivity (=B_c) as a function of grain size for 40 nm magnetite. (c) An SC plot for 40 nm grain. Uniaxial shape anisotropy dominates over magnetocrystalline anisotropy at higher elongations of $q > 1.3$.

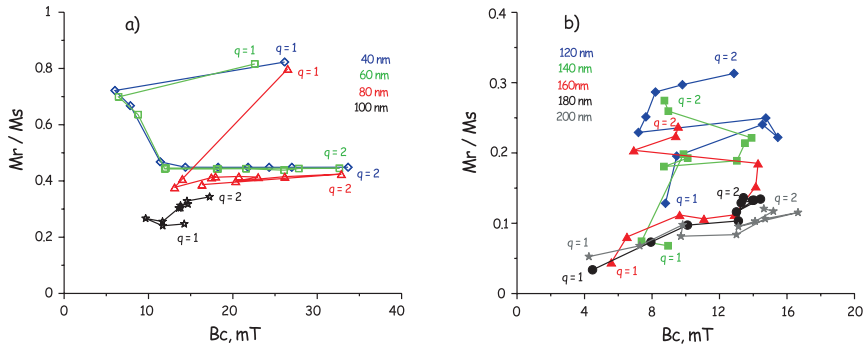

Figure 4. SC plots for (a) 40–100 nm and (b) 120–200 nm magnetites. Squareness and coercivity decrease as the grain size increases. For 100–200 nm, squareness and coercivity increase as the aspect ratio increases.

Figure 2.6] provides less costly answer. According to our calculation, hysteresis along [001], [100], and [111] has corresponding weightings of 0.1123, 0.3022, and 0.5855 in a normalized scale. On the basis of Euler angle approximation, the weighted hysteresis loop represents the hysteresis of an assemblages whose grains are randomly oriented (Figure 2d).

[19] Is Euler angle approximation necessary in micromagnetic simulation? The simulated squareness of 4 × 6 40 nm grain is 0.995, 0.000, and 0.575 along the [001], [100], and [111], respectively (Figure 2d). In this configuration, both weighted and arithmetic mean yield a squareness close to ideal SD value (Figure 2d). The simulated squareness of 4 × 5 40 nm grain is 0.93, 0.83, and 0.25 along the [001], [100], and [111], respectively. For this grain, the weighted squareness is 0.498, well representing the hallmark for the SD grain. On the other hand, a simple arithmetic mean (=0.67) yields an overestimation of the squareness, strongly suggesting that Euler angle approximation is required.

3. Simulation Results

3.1. Micromagnetic Modeling of Full Hysteresis

[20] In order to determine conventional rock magnetic parameters (M_s, M_r, and B_c), full hysteresis loops were simulated. For 40 nm magnetite, values of squareness along [111] and [100] decrease while those along [001] increase as the aspect ratio increases from 1 to 1.33, after which all the results remain nearly unchanged for q >1.4 (Figure 3a). When weighted, squareness converges at 0.45 for higher aspect ratios, which is slightly below the expected value for ideal SD grain (=0.5), indicating that averaging process somewhat underestimates the value of squareness (Figure 3a).

[21] Variation of coercivity as a function of the aspect ratio for 40 nm magnetite shows similar behavior as for squareness (Figure 3b). Values of coercivity along [111] and [100] decrease at first, then monotonically increase for $q > 1.2$ (Figure 3b). On the other hand, values of coercivity along [001] continuously increase over the entire ranges of q. Weighted coercivity shows a minimum at $q = 1.2$, then B_c continuously increases as q increases. A big difference between the variation of remanence and that of coercivity is that the turning point occurs at $q = 1.33$ for the remanence but at $q = 1.2$ for the coercivity (Figures 3a and 3b). This difference is not uncommon in micromagnetic simulation, and it poses a difficulties in predicting granulometry by using magnetic hysteresis [e.g., *Newell and Merrill*, 2000a].

[22] In a squareness-coercivity (SC) plot, hysteresis properties of 40 nm grain shows an interesting migration (Figure 3c). For cubic grains, the dominance of magnetocrystalline anisotropy is demonstrated from the value of high squareness of 0.823 (see data in Figure 3c). This is again slightly underestimated compared to the theoretic calculation of 0.866. As the aspect ratio increases, uniaxial shape anisotropy is introduced. Uniaxial shape anisotropy dominates over magnetocrystalline anisotropy at higher elongations of $q > 1.3$ (Figure 3c), agreeing well with the analytic theory [see *Tauxe et al.*, 2002].

[23] On an SC plot, a similar migration path is observed for 40–80 nm (Figure 4a). In these grains, squareness remains >0.35 at higher elongation of $q > 1.3$. For 100–160 nm grains, squareness decreases substantially (e.g., from 0.27 at $q = 2$ to 0.07 at $q = 1$ for 140 nm) as the average aspect

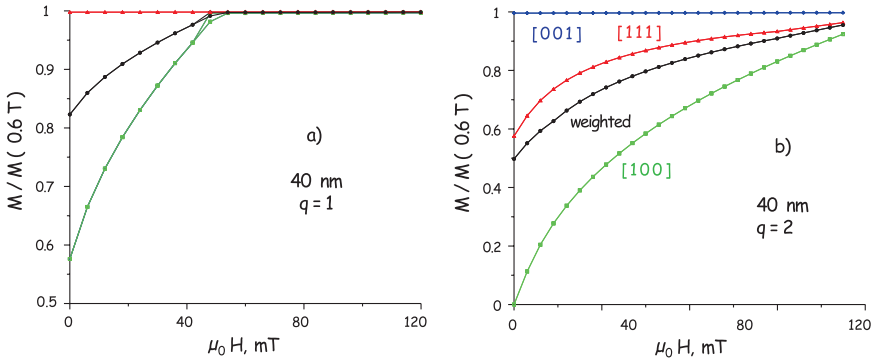

Figure 5. Micromagnetic simulation of ZFORCs for 40 nm magnetite, which virtually shows no transient hysteresis: (a) $q = 1$ and (b) $q = 2$.

ratio decreases (Figure 4). On the other hand, the variation of coercivity is confined only to 5–15 mT for 100–160 nm grains (Figure 4). Weighted hysteresis for 180–200 nm grains shows squareness of 0.04–0.13 and coercivity of 6–17 mT, typical values for small MD grains (Figure 4b). In these large grains, the transition zone of dominant anisotropy swapping is disappeared (Figure 4b).

3.2. Micromagnetic Modeling of Transient Hysteresis

[24] For a 40 nm particle of magnetite, all the ZFORCs (descending to zero from saturation magnetization, then again to saturation) are nearly reversible (Figure 5). As a result, magnetic TH is virtually absent for 40 nm grains. A very slight TH is observed along [001] and [100] for some configurations of $q = 1$ (Figure 5a), but it disappears at higher q (Figure 5b). For elongated 40 nm grain, regardless of the aspect ratio, ZFORCs remain nearly saturated along [001] but vary from near saturation to zero magnetization along [100] (Figure 5b). ZFORCs along [111] fall between them.

[25] Irreversible ZFORCs evolve as the grain size increases (Figures 6 and 7). TH for the 100 nm

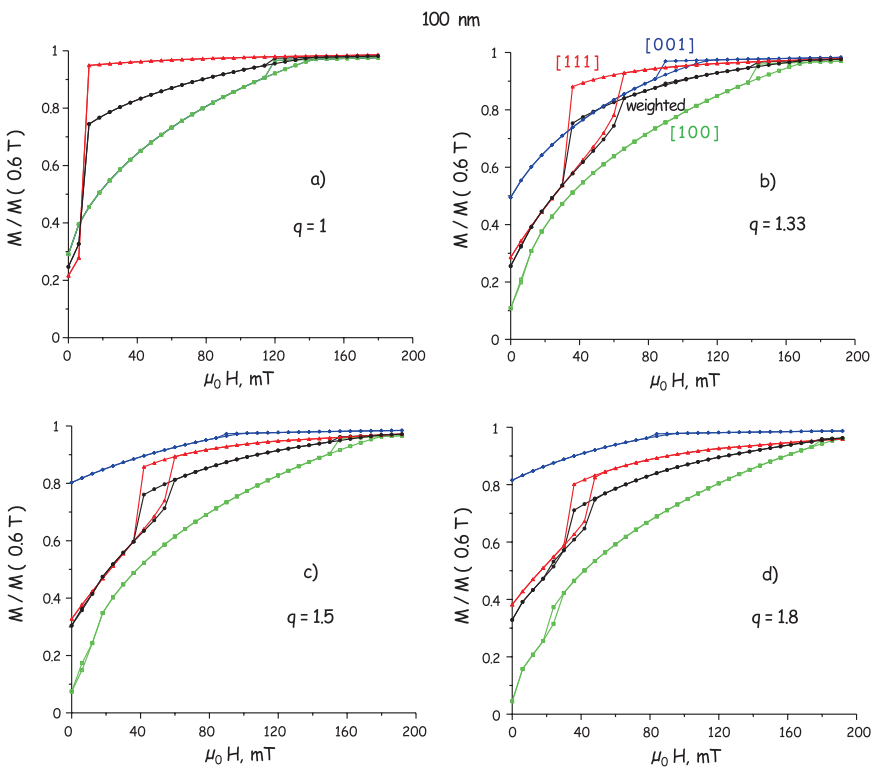

Figure 6. Micromagnetic simulation of ZFORCs for 100 nm magnetite. (a) $q = 1$, (b) $q = 1.33$, (c) $q = 1.5$, and (d) $q = 1.8$. Transient hysteresis decreases as the aspect ratio increases.

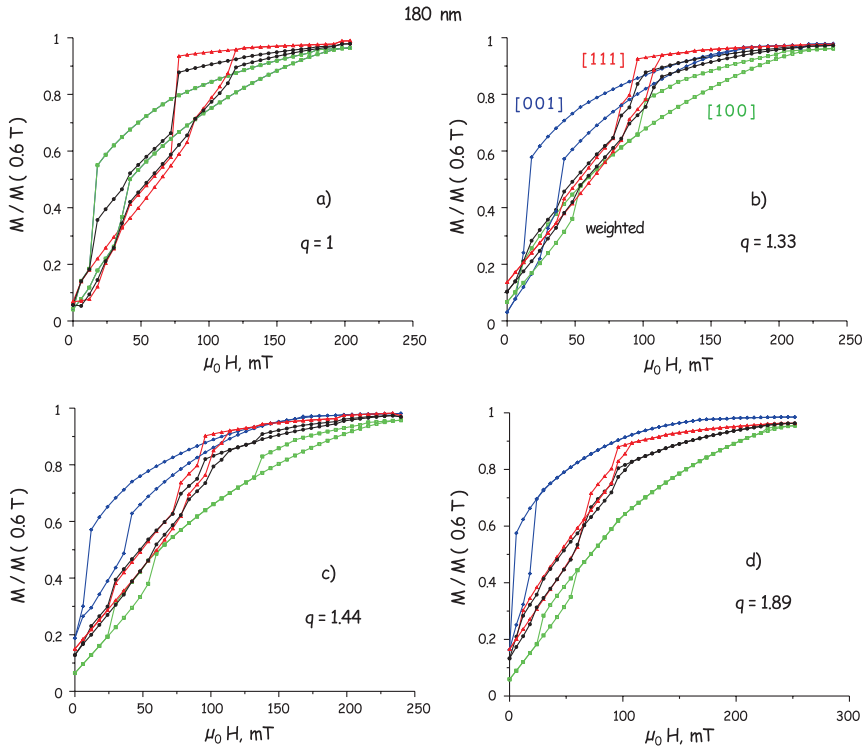

Figure 7. Micromagnetic simulation of ZFORCs for 180 nm magnetite: (a) q = 1, (b) q = 1.33, (c) q = 1.44, and (d) q = 1.89. Transient hysteresis decreases as the aspect ratio increases.

grain shows three aspects worthy of note. First, TH along [001] occurs largely at q = 1.0–1.33, but nearly disappears as q increases (Figure 6). Second, in a given configuration, TH along [111] is the largest, but it also decreases as q increases (Figure 6). Third, an irreversible ZFORCs along [100] was observed both at low (<40 mT) and high (>120 mT) applied fields (Figure 6).

[26] Results for 180 nm grains are much more complicated (Figure 7). Irreversibility is observed in all configurations and occurs over a broad range of applied fields. In particular, TH along [001] reaches a maximum at 15–20 mT, despite their small contribution on a weighted scale (Figures 7b, 7c, and 7d). In general, as in smaller grains, TH decreases as q increases (Figure 7).

3.3. Properties of Transient Hysteresis

[27] What causes transient hysteresis? In order to explore the physical basis of TH, we present snapshots of hysteresis at major turning points where TH became largest on the hysteresis curves. For graphical convenience, we will use the 100 nm grain (Figures 8–10). The first example is a comparison of magnetization vectors at $\mu_0 H$ = 90 mT for 6 × 6 × 8 configuration of 100 nm grain along [001] direction. In the descending branch, each magnetic vector remains quasi-parallel to the applied field direction (Figure 8a), showing a typical flower state of magnetization. On the ascending loop, magnetic vectors are much more curled, resulting in a reduced net magnetization (Figure 8b). However, the entire magnetization structure is still flower-like (Figure 8b).

[28] Snapshots of hysteresis along [100] show quite different behavior. The difference of magnetization structure between the descending and ascending loops is less significant with both being curled. For an applied field of $\mu_0 H$ = 24 mT, there is only a slight difference of magnetization vectors near the bottom-right edges (Figure 9).

[29] A distinct contrast between a more flower-like structure (Figure 10a) and a vortex-like structure (Figure 10b) is observed for the snapshots of hysteresis at $\mu_0 H$ = 42 mT for a 100 nm grain of 6 × 6 × 8 configuration along the [111] direction. This fundamental difference of magnetic structures is responsible for the great difference of their magnetization, hence irreversible ZFORC behavior, or TH.

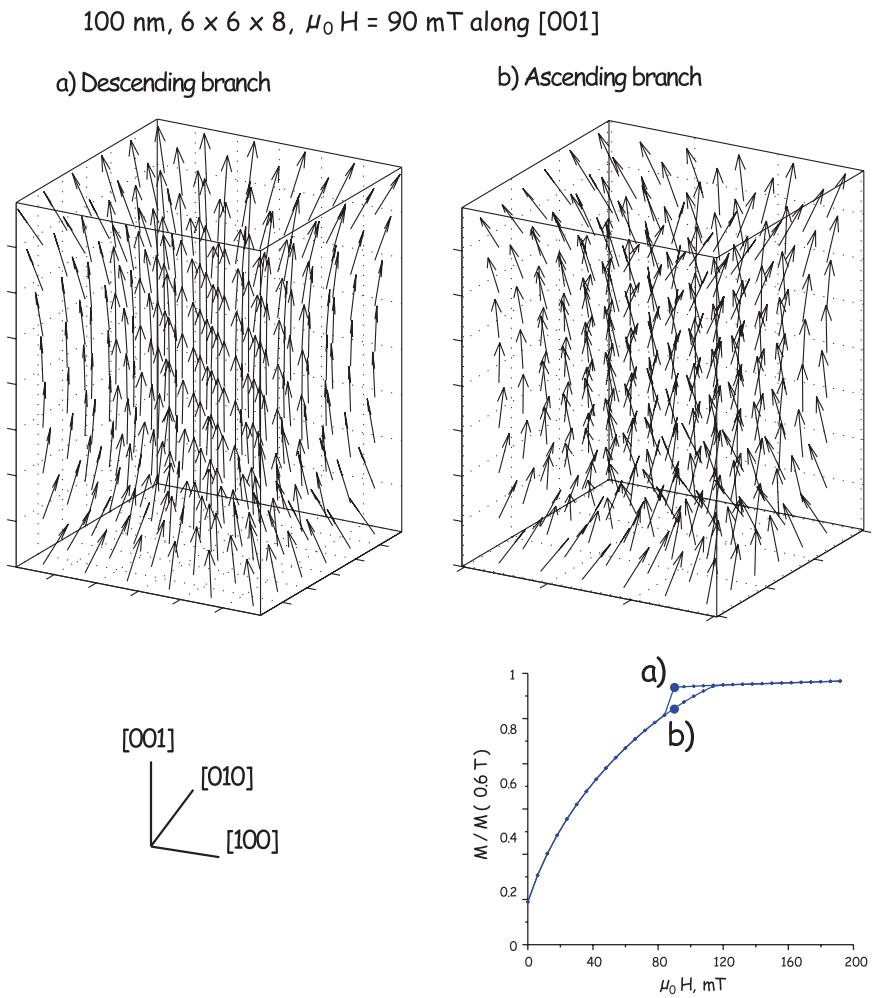

Figure 8. Snapshots of magnetization configuration at $\mu_0 H$ = 90 mT along [001] for 6 × 6 × 8 100 nm magnetite: (a) descending branch and (b) ascending branch. Note that magnetic vectors are more curled in the ascending branch.

[30] On the basis of these snapshot analyses, we can conclude that TH results from the difference of magnetization structures between the ascending and descending loops. A much more uniform, higher magnetization state (e.g., flower-like) is preferred for the descending branch, while a more complicated, lower magnetization state (e.g., vortex-like) is common for the ascending branch (Figures 8–10). This contrast is most prominent along the [111] direction, giving rise to transient hysteresis.

3.4. Grain Size Dependence of Transient Hysteresis

[31] Because transient hysteresis in the zero-FORC experiment originates from the action of self-demagnetization, it should increase as grain size increases and as the average aspect ratio decreases. Indeed, transient hysteresis is nearly absent for 40 nm and 60 nm (e.g., Figure 5). In these grains, TH is virtually zero for all the configurations of the simulated aspect ratio. Although there are a few occasions (particularly for q < 1.3) where minor TH events occur, TH would be undetectable in practice due to the small value (<1% difference of saturation magnetization).

[32] For magnetite particles of 80–140 nm, TH along the [111] dominates in weighted results, peaking at 25–65 mT (e.g., Figure 11a). TH for 100 nm magnetite fits well with the prediction, decreasing as q increases (Figure 11b).

[33] Properties of TH for 180 nm magnetite particles are complicated. Despite their small weighting factors, TH along [001] and [100] often

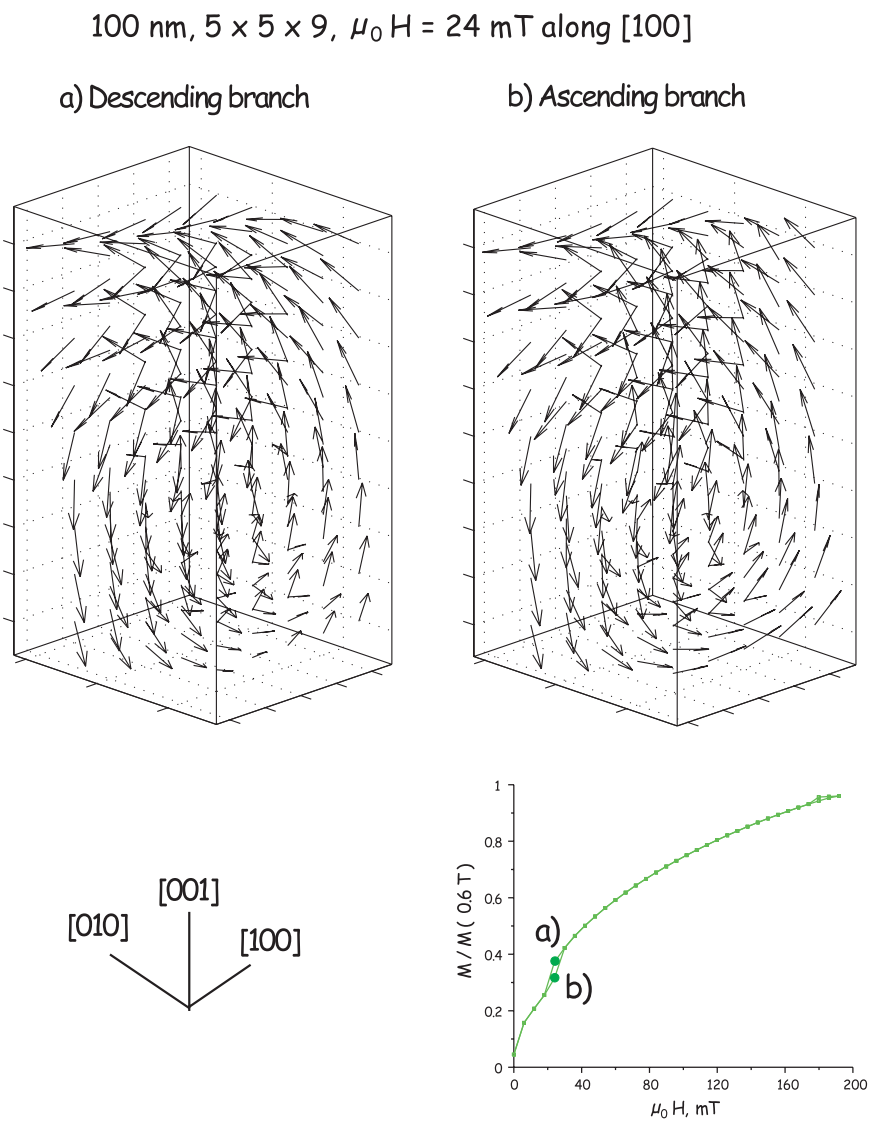

Figure 9. Snapshots of magnetization configuration at $\mu_0 H = 24$ mT along [100] for $5 \times 5 \times 9$ 100 nm magnetite: (a) descending branch and (b) ascending branch. There exists a slight difference of magnetization vectors near the bottom right edges.

shows peaks at higher applied fields >120 mT (Figure 11c). As in other grains, TH along [111] dominates on a weighted scale, being most prominent at smaller applied fields <120 mT (Figure 11d). Although not shown, a similar behavior was observed for 160 and 200 nm grains. In general, regardless of the size of the grain, TH decreases as the q increases (Figure 11).

4. Experimental Observations

[34] In order to compare our numerical experiments to "real" data, we have carried out a number of hysteresis experiments on magnetite assemblages of carefully sized powders as well as natural materials. These are described in the following sections.

4.1. Samples and Experiments

[35] Six synthetic powders were studied whose mean grain sizes range from SD (65 nm) to small MD (18.3 μm). A brief summary of sample properties is presented in Table 1 (see *Yu et al.* [2002] for a detailed sample description). For each grain size, three sets of powders were prepared. The first set of powders was 0.5% by volume dispersions of magnetite in a matrix of CaF_2. These were vacuum-sealed in quartz capsules of 3 cm and annealed

Table 1. Synthetic Samples[a]

Powder	d, μm	q (Axial Ratio)	n
4000	0.065	1.48	884
Mapico	0.24	1.29	532
112978	0.44	1.33	1022
3006	1.06	1.62	1471
112982	16.9	1.61	1618
041183	18.3	1.57	870

[a] Powders 4000, 112978, 3006, 112982, and 041183 are from the Wright Company. Powder Mapico is the products of Mapico Company. d is the estimated grain size, q is the average axial ratio, and n is the number of grains counted. Size distribution was determined by counting individual grains from at least six different SEM photos per powder. See *Yu et al.* [2002] for details.

for 3 hr at 973 K to stabilize the magnetic properties. After annealing, the samples were slowly cooled from 973 K because rapid quenching may result in higher thermal stresses. The quartz capsules were unsealed just prior to the hysteresis measurements. The second set of powders was 0.5% volume dispersions of unannealed magnetite in a matrix of CaF_2. The third set consists of undispersed, pure magnetite powders.

[36] Natural samples were also studied: 456H (lake sediments, Lake Pepin, Minnesota, USA [*Brachfeld and Banerjee*, 2000]); E0–E5 (zero-age mid-oceanic ridge basalts, from the East Pacific Rise [*Gee and Kent*, 1997]); KM3C-F (Kometsuka basalts, Mt. Aso, Japan [*Yu*, 1998]); P0–P3 (MORBs, Phoenix expedition, from the East Pacific Rise [*Gee and Kent*, 1999]); and TG2, TG19D (Tudor Gabbro, Ontario, Canada [*Yu and Dunlop*, 2001]). On the basis of previous studies, we selected individual chips whose sister chips yielded hysteresis ratios falling in various regions in the Day plot [*Day et al.*, 1977], spanning the range from SD, PSD, MD, and SP (Table 2). In particular, E0–E5 represent subsamples spaced every 5 mm with respect to the outer chilled margin of a single pillow lava with E0 representing a subsample nearest the chilled margin.

[37] Room temperature hysteresis was measured by using the alternating gradient force magnetometer (AGFM) at Scripps. ZFORCs and full hysteresis loops were monitored in the peak field 0.5 T in field increments/decrements of 5 mT. The signal averaging time was usually set to 500 ms, but 1 s was used for weak samples.

4.2. Synthetic Samples

[38] When we plotted TH as a function of grain size, submicron magnetites display the expected grain size dependence; as the grain size increases, TH increases (Figures 12a and 12b). For each grain size, TH is largest for the annealed set and smallest for unannealed bulk magnetites (Figures 12a and 12b). For comparison, we also plotted the predicted TH from the micromagnetic modeling (Figure 12a). Because of the high computation demand, most simulations covered only the lower end of the grain size range (40–200 nm). The range of TH varies substantially for different simulations but agrees reasonably well with the experimental results for q = 1.5 (Figure 3a). Note that the average aspect ratio of the synthetic magnetites was about q = 1.5 (Table 1). Substantially higher values of TH from some simulations belong to near cubic grains (q < 1.3) of magnetite, which is usually less common in most natural or synthetic samples.

[39] For comparison, we display our results in a conventional Day diagram (Figures 12c and 12d). In the Day diagram, the ratio of hysteresis parameters for each set of grain sizes migrates toward the MD end as the volume concentration decreases and as the annealing is performed (Figures 12c and 12d). This trend is universally true regardless of the grain size of magnetites.

[40] The 65 nm magnetite shows squareness of 0.2–0.32 (Figure 12c), substantially lower than expected value 0.5 of ideal SD. However, a rather small TH is observed compared to other submicron magnetites (Figures 12a and 12b), indicating that low squareness results from the unblocking of SP grains and not from the PSD/MD grains. It is worthy of note that TH is unexpectedly small for 16.9 and 18.3 μm magnetites (Figure 12b).

[41] For synthetic samples of all grain sizes, annealed samples yielded the smallest squareness but the largest TH, suggesting that annealing encourages a more MD-like nature of the grains (Figures 12). For the unannealed set of submicron

Table 2. Natural Samples[a]

Sample	References	T_{UB}, °C
Kometsuka Basalt	1	500–560
Lake Pepin Sediments	2	580
MORBs, Phoenix expedition	3	160–360
Tudor Gabbro	4	580
Zero-age MORBs, East Pacific Rise	5	80–120

[a] T_{UB} is the maximum unblocking temperatures from the thermal demagnetization of sister specimens. References: 1, *Yu* [1998]; 2, *Brachfeld and Banerjee* [2000]; 3, *Gee and Kent* [1999]; 4, *Yu and Dunlop* [2001]; 5, *Gee and Kent* [1997].

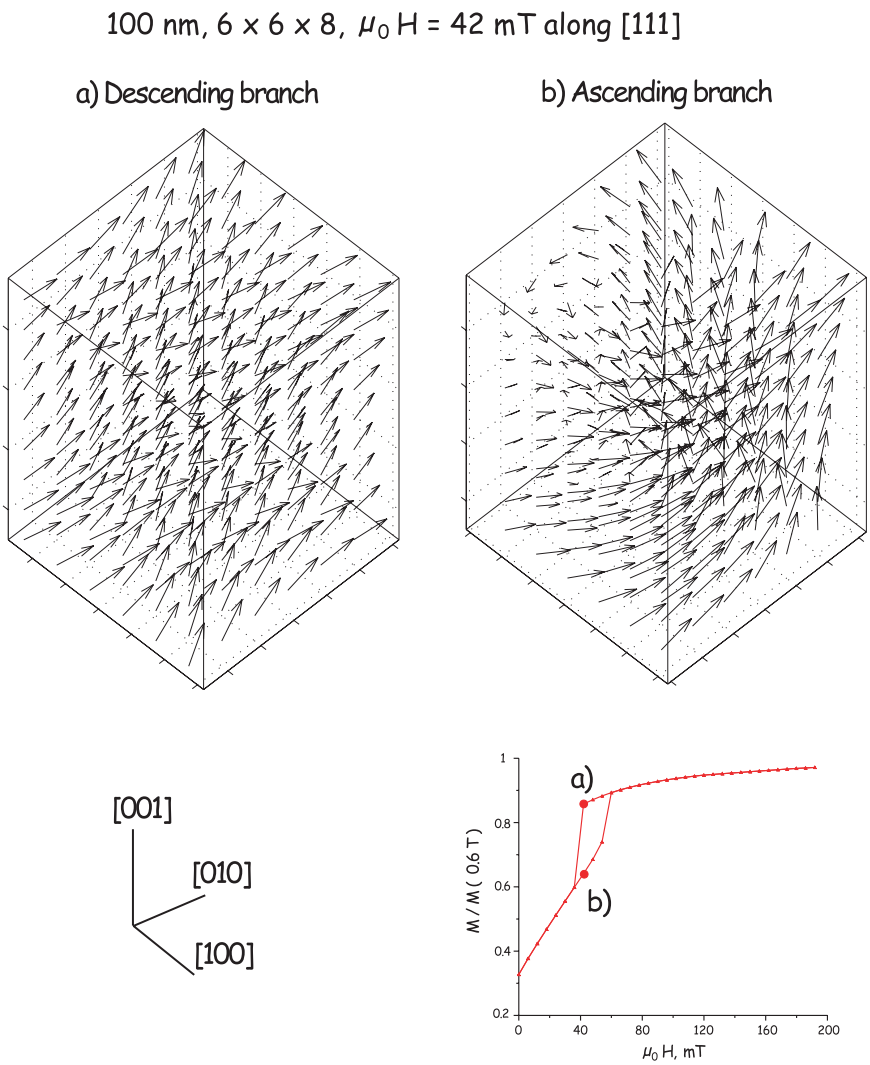

Figure 10. Snapshots of magnetization configuration at $\mu_0 H = 42$ mT along [111] for $6 \times 6 \times 8$ 100 nm magnetite: (a) descending branch and (b) ascending branch. While the descending branch shows a more uniform (flower-like) structure, the ascending branch shows a less uniform (vortex-like) configuration.

magnetites, an increase of volume concentration enhances squareness but reduces TH (Figure 12). Although a similar trend is observed for 18.3 μm, a difference in volume concentration makes little impact on squareness (Figure 12).

4.3. Natural Samples

[42] All the experimental results are displayed on three separate plots (Figure 13). We examined the relation between squareness and TH along with a Day diagram and a squareness-coercivity (SC) plot for comparison. In Kometsuka basalts, KM3F shows ideal SD behavior with a squareness of 0.5 (Figures 13a, 13b, and 13c). KM3C shows enhancement of TH with smaller squareness, possibly resulting from increasing grain size of (titano)magnetite. The two Tudor gabbros and one lake sediment sample apparently fall in the so-called PSD-MD range in Day plot (Figure 13a). However, they have distinctively different TH (Figure 13c). T2C shows typical MD characteristics with substantial TH and a fairly low squareness of 0.05 (Figure 13c). In contrast, T19D shows minimal TH while having relatively low squareness of 0.24, suggesting the presence of SP as opposed to MD particles (Figures 13a, 13b, and 13c). The 456H falls between them.

[43] For MORBs, E2 (1 mm from the chilled margin respectively) show SD behavior with high squareness and minimal TH (Figures 13d, 13e, and 13f). Apparently, E2 and E3 show similar squareness, but their THs are quite different,

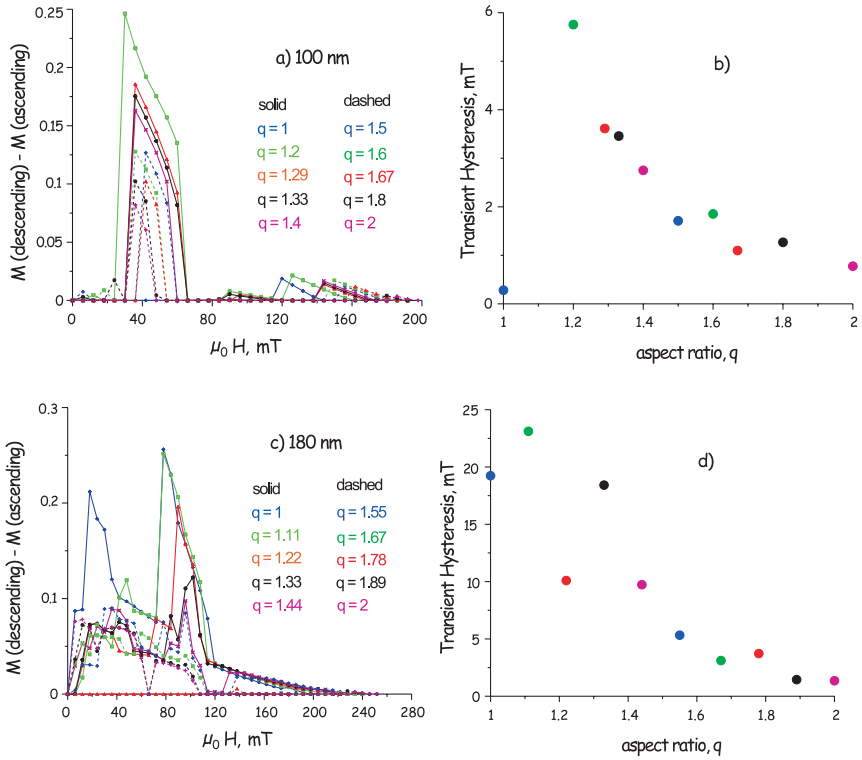

Figure 11. (a) Difference of magnetization between descending and ascending magnetization for 100 nm magnetite. (b) Estimated transient hysteresis as a function of axial ratio. Transient hysteresis decreases as the average aspect ratio increases. (c) Difference of magnetization between descending and ascending magnetization for 180 nm magnetite. (d) Estimated transient hysteresis as a function of axial ratio. Transient hysteresis decreases as the average aspect ratio increases.

indicating the presence of relatively coarse grains in E3 (Figures 13d, 13e, and 13f).

5. Discussion

[44] Magnetic hysteresis has been used as a standard procedure in rock and environmental magnetism to estimate domain states, by implication, average grain size of remanence carriers. One of the most difficult tasks for paleomagnetists is the clear distinction between SP and PSD/MD when the results fall in the so-called PSD region in the Day plot. In ideal SD grains, squareness is high (0.5 for uniaxial anisotropy). However, low squareness occurs for PSD/MD due to both domain wall formation resulting from self-demagnetization effect and to SP behavior owing to thermal agitation. Although SP tends to fall in a somewhat different region (toward upper right portion in the Day plot [e.g., *Tauxe et al.*, 1996]), a clear cut distinction of SP and PSD/MD in the Day plot is often ambiguous [e.g., *Gee and Kent*, 1999; *Dunlop*, 2002a, 2002b; *Tauxe et al.*, 2002]). The SC plot offers some advantages over the Day plot in displaying the temperature dependence of hysteresis and in recognizing dominant anisotropy of remanence carriers, yet it requires fewer measurements [*Tauxe et al.*, 2002; *Yu et al.*, 2004]. However, the SC plot also cannot clearly discriminate SP from PSD/MD (e.g., Figures 13b and 13e). The TH experiment was designed to better diagnose these ambiguities [*Fabian*, 2003].

[45] In this study, we have tried to provide a physical rationale for the use of TH in granulometry by using micromagnetic simulation. TH results from the action of self-demagnetization which causes irreversible paths in the ZFORCs (Figures 5–7). TH is largest along [111] but smallest along the elongation direction [001] (Figures 6 and 7). It is interesting that TH develops both at low- and high-field regions along [100] (Figures 6 and 7). Whenever there is an irreversibility, regardless of the applied field direction, the magnetization configuration for the descending branch favored a more uniform (e.g., flower-like) structure while that for ascending branch preferred less uniform

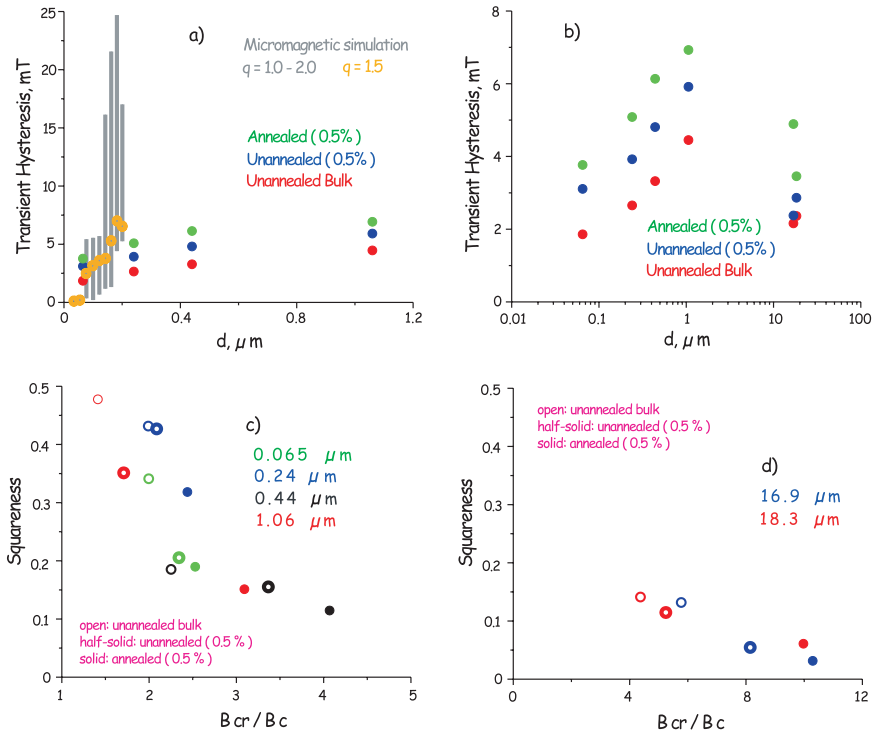

Figure 12. (a) Comparison of grain size dependence of TH for synthetic magnetites and for micromagnetic simulation. TH from the simulation for samples with aspect ratio q = 1.5 agrees well with the experimental observations for annealed magnetites. (b) Grain size dependence of TH for synthetic magnetites. Day diagrams for synthetic magnetite: (c) submicron magnetites and (d) small multidomain magnetites.

(e.g., vortex-like) structure (Figures 8–10). This contrast was most prominent along [111], along which TH was the largest (Figure 10). Along [001] and [100] directions for higher aspect ratio q > 1.3, the magnetization structure was slightly different while maintaining a similar configuration, resulting in less significant TH (Figures 8 and 9).

[46] In general, according to our micromagnetic simulation, TH increases as the grain size increases (Figure 12a) and as the aspect ratio decreases (Figure 11). At a given grain size, TH varies substantially depending on the aspect ratio, but tends to be fairly large for smaller aspect ratio of q < 1.3 (Figure 11). In particular, TH from the simulation for q = 1.5 agrees well with the experimental observations for annealed magnetites that are relatively stress-free (Figure 12a). Note that our simulation neglected magnetoelastic effects.

[47] For volcanic rocks and sediments, TH is minimal for samples containing SP grains (e.g., T19D in Figure 13c). For most samples, squareness decreases as TH increases, along with an increase in the average grain size. The only exception was the T19D which has SP grains (Figure 13c).

[48] Results of oceanic basalts are much more complicated. As the distance from the chilled margin increases, hysteresis ratios in the Day diagram and SC plot migrate in counterclockwise path (Figures 13d and 13e). In fact, the reduced remanence ratio near chilled margin was explained as a result of SP unblocking [*Gee and Kent*, 1999]. In a plot of squareness versus transient hysteresis (S-TH), we confirm the earlier interpretation of *Gee and Kent* [1999] by showing minimal TH for E0 (Figure 13f). As we penetrate toward the interior, for the first several mm, the SP fraction decreases while the average grain size reaches a stable SD size, apparently increasing squareness yet not affecting TH much because ideal SD as well as SP lacks the TH. As the distance from the margin exceeds 1 cm, the increase of magnetic grain size is demonstrated from the fact that squareness decreased and TH increased, as the grains reached so-called PSD size (Figure 13f). Of course, a change of mineralogy should be considered as well [see *Gee and Kent*, 1999; *Wang and Van der Voo*, 2004].

[49] In the original paper, *Fabian* [2003] used a ratio of TH/FH, which is the ratio between the area

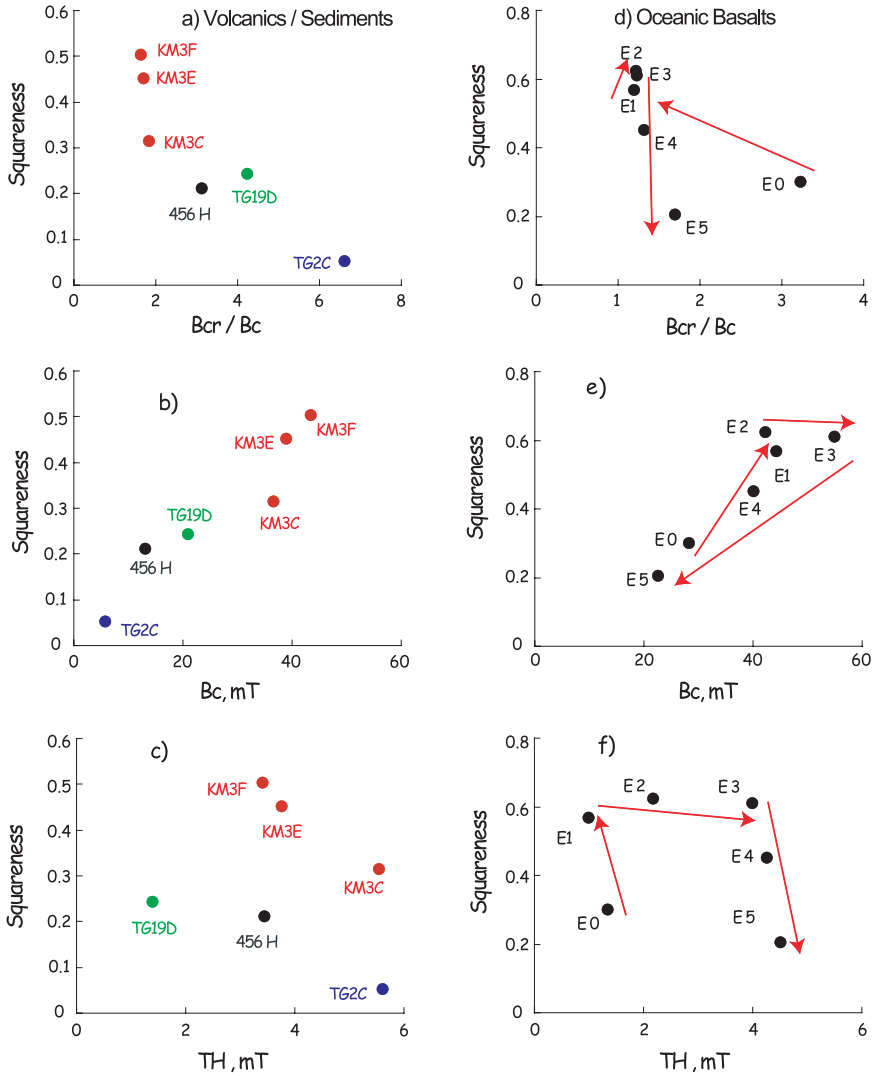

Figure 13. Day diagrams, SC plots, and squareness versus TH plots (STH plots) for natural samples. (a–c) Volcanics/sediments and (d–f) MORBs. Discriminating SP from PSD/MD is clearly diagnosed in STH plots.

of TH and that of full hysteresis (FH). However, this ratio is mostly controlled by the denominator term. As a result, the excellent grain size dependence of TH/FH of *Fabian* [2003] overshadows the actual properties of TH. In fact, according to our observations, TH itself shows a linear grain size dependence only for submicron magnetites (Figure 12a). It is somewhat surprising that TH is not the largest for MD samples (Figure 12b).

[50] How can >10 μm magnetite show less TH than submicron magnetite? Because the TH results from the action of self-demagnetization, we anticipated that TH would increase as the grain size increases. However, "real" MD grains would have very little hysteresis because it is nearly completely demagnetized in the remanent state (near-zero squareness). In other words, TH would increase as the grain size increases over certain grain size ranges but it must decrease once there are several domain walls. On the basis of our experimental observation, TH begins to decrease when the average particle size exceeds 1 μm (Figure 12b). Nonetheless, it is apparent that TH is sensitive in detecting 1 μm magnetite, suggesting that TH can be used as a granulometric proxy in environmental magnetism.

[51] Our simulations indicate that the difference of magnetic structures between ascending and descending branches is responsible for TH. We found that the ascending branch always forms less uniform (vortex-like) structures, thus have lower magnetizations. Perhaps, TH signals the difference between the vortex or flower state (descending) and two domains (ascending) of 1 μm and the

difference between four domains (descending) and eight domains (ascending) of 18.3 μm, yielding greater TH for 1 μm magnetite. In this case, the difference of magnetization for 1 μm would be much larger than that for 18.3 μm magnetite. Note that earlier microscopic observations/compilation for titanomagnetite [e.g., *Halgedahl and Fuller*, 1983; *Appel and Soffel*, 1985] and for magnetite [e.g., *Geiss et al.*, 1996; *Özdemir and Dunlop*, 1997] show that 1 μm grains seldom display more than two domains, while >10 μm grains show several domains. However, this proposition requires further testing because the micromagnetic analysis and microscopic observations cover only a limited grain size (Figure 12).

[52] How well can TH distinguish SP from PSD in practice? Direct comparison of squareness provides no clear distinction between SP and PSD (Figures 12 and 13). In fact, results in Figures 12 and 13 clearly show that using squareness alone in granulometry is risky. In order to better diagnose the domain state of remanence carrier, we need an additional parameter. Measuring TH serves the purpose. For example, magnetic granulometry of MORBs that are deduced from traditional Day plots incited much debate [e.g., *Gee and Kent*, 1997, 1999; *Xu et al.*, 1997; *Tauxe et al.*, 2002]. The trend of increasing grain size as the distance from the chilled margin increases is best displayed in STH plot (Figure 13f). The presence of SP is best diagnosed in an STH plot, where TH is zero for SP. In conclusion, a very small TH is a clear indication for the SP or ideal SD particles (Figures 13c and 13f).

[53] However, a true MD also shows a negligible MD due to its near zero magnetic remanence. Hence we need additional rock magnetic information (e.g., frequency-dependence of magnetic susceptibility) or microscopic observation to fully distinguish SP from MD.

6. A Preisach Formalism

6.1. A Classical Preisach Model

[54] In a classical Preisach model [*Preisach*, 1935], the magnetic material is composed of elementary domains that independently switch magnetic moments from M^+ to M^-, or vice versa. The Preisach model can be decomposed into the switching fields which set the magnetization up (H^+ for M^+) or down (H^- for M^-) depending on the direction of the magnetic field H. In a given state, by increasing H, the elementary domains that have magnetizations along H^- (whose critical switching field (H_{crit}) is $\leq H$) reverse their directions to H^+. Conversely, with decreasing magnetic field, domains whose $H_{crit} \geq H$ also reverse their direction of magnetization. A fundamental underlying assumption is that each domain possesses two switching fields (H^+ and H^-). If so, the same set of domains will be magnetically activated between any pair of switching fields. This interesting assumption has been validated in various magnetic systems, known as the properties of congruency and wiping-out return memory [e.g., *Bertotti*, 1998].

[55] In a classical Preisach model, the distribution of switching fields $f(H^+, H^-)$ is defined so as to incorporate the changes of the switching fields. For example, $f(H^+, H^-)\Delta H^+\Delta H^-$ is proportional to the number of domains that have M^+ in an infinitesimal range around H^+ and a M^- in an infinitesimal range around H^- [e.g., *Bertotti*, 1998].

[56] This description of the magnetization process is equivalent to the concept of Barkhausen jumps where the magnetization of domains abruptly switch their polarity at the threshold fields. The Preisach diagrams are a convenient tool to display such a process and switching fields involved in a magnetic system. The fundamental drawback of the Preisach approach is the need for a distribution function to describe the hysteresis loop. In fact, the exact distribution function is available only from the experimental determination [e.g., *Dunlop and West*, 1969].

6.2. A Modern Preisach Model

[57] A modern Preisach model [e.g., *Boots and Schep*, 2000; *Metlov*, 2000; *Song and Roshko*, 2000; *Song et al.*, 2001; *Borcia et al.*, 2002] includes a free energy landscape (regardless of the complexity) that is an ensemble of bistable subsystem components. Each bistable component has two stable states with a corresponding pair of energy barriers, W^+ and W^-. For example, we present a simple model of a bistable system whose energy barriers are equivalent to $W^+ = -Mb$ and $W^- = Ma$ (Figure 14a). These energy barriers inhibit transitions from one energy minimum state to the other, or vice versa. In a given relation, the coercivity and asymmetry field can be represented as $h_c = (W^+ + W^-)/2M$ and $h_i = (W^+ - W^-)/2M$, respectively (Figure 14a).

[58] On the basis of a bistable decomposition, any given magnetic system can be characterized by a

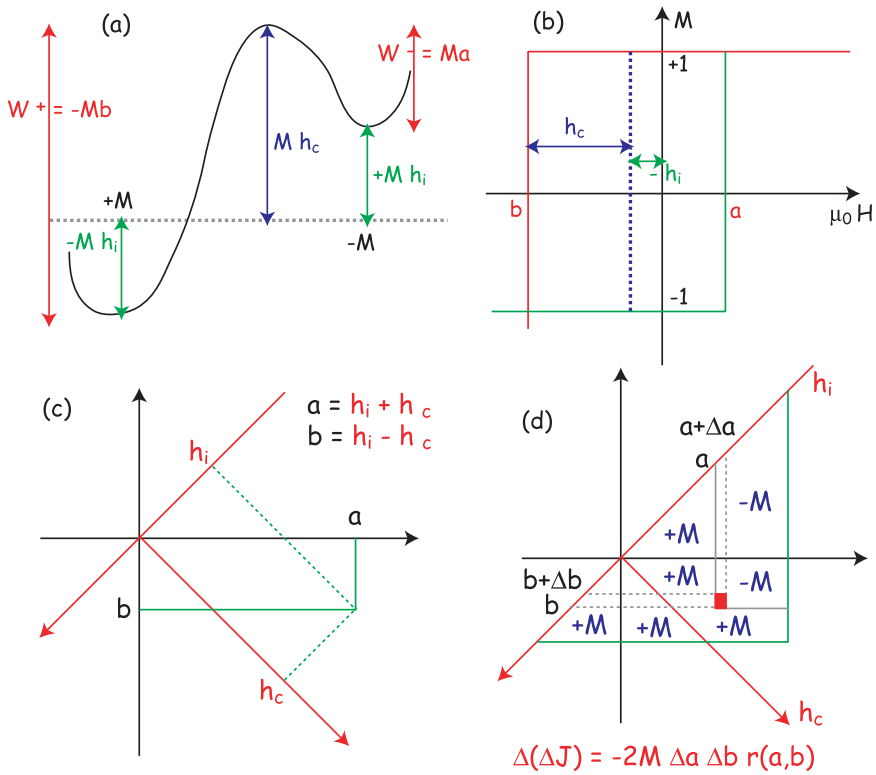

Figure 14. (a) A free energy profile for a cluster with two stable moments: h_c, intrinsic coercivity; h_i, interaction field. (b) A hysteresis for the cluster of Figure 14a with critical switching fields a and b. (c) The Preisach plane showing the relation between switching fields (a, b) and coercivity/interaction field (h_c, h_i). (d) A representation of the Preisach density.

particular distribution $f(W^+, W^-)$ of free energy barriers, or equivalently by a distribution of the switching fields, $f(h_c, h_i)$ or $f(a, b)$. In principle, the Preisach diagrams represent the distribution of $f(a, b)$ while the first-order reversing curve (FORC) diagrams [e.g., *Pike et al.*, 1999] represent the distribution of $f(h_c, h_i)$.

[59] Transitions between different energy minima states occur when enough energies (whether external field or thermal excitation) are supplied. For instance, the presence of the external field H_a shifts the energy state of the M_+ by $-MH_a$, and the energy state of M^- by $+MH_a$ (Figure 14b). As a result, the external field H_a modifies the entire system by amount of MH_a (Figure 14b).

[60] Each subsystem and its instabilities can be graphically displayed in the Preisach plane (Figure 14c), which uses the characteristic fields (a, b) and (h_c, h_i) to define rectangular coordinates axes. Each subsystem is represented by a point in this plane, and the distribution of subsystem is described by a probability density $\rho(h_c, h_i)$ or $\rho(a, b)$ (Figure 14d). In a physical sense, a change in a magnetic system can be represented as the shaded area confined by an increment/decrement of a and b (Figure 14d):

$$\Delta(\Delta J) = [-2M\Delta a\Delta b]\rho(a, b). \quad (5)$$

This area is equivalent to the energy dissipated or stored in a system (Figure 14d) in a subsequent irreversible changes (Barkhausen jumps). Inversely, the probability density $\rho(a, b)$ is equivalent to

$$\rho(a, b) = -\partial^2 J/[-2M\partial a\partial b]. \quad (6)$$

The Preisach description has been often simplified by factorizing all the contributing factors into an independent variable [e.g., *Dunlop and West*, 1969; *Bertotti*, 1998; *Song and Roshko*, 2000; *Song et al.*, 2001]. This type of factorization is valid when we are dealing with individual physical entities, such as magnetic particles or domains.

6.3. First-Order Reversal Curves

[61] It has been demonstrated that FORC diagrams are a useful diagnostic tool in interpreting the hysteresis properties of magnetic materials [e.g., *Pike et al.*, 1999; *Roberts et al.*, 2000]. In order to

obtain a given FORC, samples are first saturated in a positive field (+H), then they are ramped down to a reversal field H_a. The FORC consists of a series of magnetic measurements as the field is increased from H_a to the saturation. In a given specific magnetic field of H_b ($H_b > H_a$), the FORC with a reversal point H_a is denoted as $J(H_a, H_b)$. A FORC distribution is defined as

$$\rho(H_a, H_b) = -\partial^2 J(H_a, H_b)/[\partial H_a \partial H_b]. \quad (7)$$

In order to construct a FORC distribution $\rho(H_a, H_b)$, a polynomial best-fit is calculated from the sequential data points in an arbitrary array of the measured reversal curves. In other words, the FORC distribution is not unique, and is strongly subjective as to the choice number of data points (which is proportional to the smoothing factor).

[62] In a physical sense, the FORC density represents the difference of the slope at each magnetic field (H_b) along the different reversing curves. As a result, the FORC diagram illustrates the probability of the irreversible changes in a magnetic system. As *Néel* [1954] supposed, only two physical situations are compatible with the Preisach approach: interacting SD particles and a planar domain wall in a randomly distributing dislocations. In these ideal situations, the Preisach density truly represents the distribution of microcoercivity and interaction fields. On the basis of the analogy between the Preisach and FORC diagrams, it has been traditionally suggested that FORCs represent the distribution of microcoercivity and interaction. Unfortunately, most useful magnetic grains in rocks are not interacting SD or MD with domain walls. Instead they contain grains whose magnetization states are so-called "PSD", vortex, and/or flower structures. In a FORC analysis, the FORC diagram displays the distribution of Barkhausen jumps (microcoercivities), or other changes in magnetic states (e.g., change from vortex to flower). In other words, the FORC diagrams can reasonably represent the distribution of microcoercivity along (H_a), but a distribution along (H_b) may result from a true interaction or from a simple change of magnetization state (e.g., vortex to flower), suggesting that labeling (H_b) as to "interaction" in FORC diagrams is a misleading simplification.

6.4. Magnetic Transient Hysteresis: ZFORC

[63] Magnetic hysteresis has been commonly used to characterize magnetic mineralogy and domain state in paleomagnetic research. In rock and environmental magnetism, an SC plot uses squareness and coercivity from the hysteresis loops and the Day plot requires an extra backfield measurements for B_{cr} determination. Conventional hysteresis measurements have recently been extended to include FORCs [e.g., *Pike et al.*, 1999; *Roberts et al.*, 2000]. Although FORC analysis offers some advantages in deciphering grain interactions, their universal application is still far from straightforward.

[64] The TH is equivalent to a single FORC, what we have denoted as ZFORC or zero FORC. Because TH measures only one reversing curve, the FORC density (or the Preisach density by implication) cannot be determined. According to our numerical simulation, the difference of magnetic structures between ascending (vortex-like) and descending (flower-like) loops is responsible for TH (Figures 8–10). The observed properties of magnetic TH can be understood by a Preisach-analog formalism as follows. It is feasible that the two different magnetization configurations constitute the bistable systems. Depending on the initial states, whether the field was increased or decreased, the entire free energy of the magnetic system falls into two different energy minima (e.g., Figure 14a). When the external field energy ($-\mu_0 M H$) is larger than W^-, the system is entirely reversible (or at least it stays in one configuration throughout the entire FORC) yielding zero TH. On the other hand, for the intervals where the external field energy ($-\mu_0 M H$) is less than W^-, the energy barriers inhibit free transformation. In this frozen bistable configuration, TH evolves due to an irreversible jump.

[65] In terms of experimental loads, the conventional Day diagram and FORC analysis require about 10 min. and several hours, respectively. Measuring TH can easily be added to the traditional hysteresis loop measurements and requires only 1–2 minutes, yet it clearly provides more useful information than what the Day plot and FORC analysis offer, an SC plot with TH analysis (combined work load of 3–5 min.) seems to be a plausible combination in the future paleomagnetic granulometry.

7. Conclusions

[66] 1. In order to provide a fundamental rationale for the use of TH in paleomagnetism as a granulometric indicator, we have carried out micromag-

netic simulations. We observed that magnetic TH results from the difference of magnetization configuration between ascending and descending hysteresis loops as a result of self-demagnetization.

[67] 2. The descending branch has a tendency to keep a more uniform (e.g., flower-like) configuration while ascending branch prefers a less uniform (e.g., vortex-like) structure.

[68] 3. We found that the TH increases as the grain size increases and as the aspect ratio decreases.

[69] 4. Results from TH simulation for samples with aspect ratio q = 1.5 agrees well with the experimental observations for annealed synthetic magnetites of smaller sizes.

[70] 5. The trend of increasing grain size as the distance from the chilled margin increase in MORBs is confirmed from the TH measurements.

[71] 6. In general, small TH is a clear indication for the absence of complex magnetized structures. Adding TH analysis to conventional hysteresis analysis requires a minor effort, yet provides a powerful constraint on grain size.

Acknowledgments

[72] Jeff S. Gee and Stefanie Brachfeld generously donated a large collection of MORBs and lake sediments for use in this study, respectively. We thank Neil Bertram, Roy M. Roshko, and Andrew Newell for valuable discussions. Wyn Williams, Qingsong Liu, and Dennis Kent provided helpful reviews. This research was supported by NSF grant EAR0229498 to L. Tauxe and N. Bertram.

References

Appel, E., and H. C. Soffel (1985), Domain state of Ti-rich titanomagnetites deduced from domain structure observations and suceptibility measurements, *J. Geophys. Res.*, *56*, 121–132.

Arfken, G. B., and H. J. Weber (1995), *Mathematical Methods for Physicists*, Elsevier, New York.

Bertotti, G. (1998), *Hysteresis in Magnetism*, Elsevier, New York.

Bertram, H. N., and G. J. Zhu (1992), Fundamental magnetization processes in thin-film recording media, *Solid State Phys.*, *46*, 271–371.

Boots, H. M. J., and K. M. Schep (2000), Anhysteretic magnetization and demagnetization factor in Preisach models, *IEEE Trans. Magn.*, *36*, 3900–3909.

Borcia, I. D., L. Spinu, and A. Stancu (2002), Simulations of magnetization curves with Preisach-Néel models, *J. Magn. Magn. Mater.*, *242–245*, 1034–1037.

Brachfeld, S. A., and S. K. Banerjee (2000), A new high-resolution geomagnetic relative paleointensity record for the North American Holocene: A comparison of sedimentary and absolute intensity data, *J. Geophys. Res.*, *105*, 821–834.

Carvallo, C., A. R. Muxworthy, D. J. Dunlop, and W. Williams (2003), Micromagnetic modeling of first-order reversal curve (FORC) diagrams for single-domain and pseudo-single-domain magnetite, *Earth Planet. Sci. Lett.*, *213*, 375–390.

Day, R., M. Fuller, and V. A. Schmidt (1977), Hysteresis properties of titanomagnetites: Grain size and composition dependence, *Phys. Earth Planet. Inter.*, *13*, 260–267.

Dunlop, D. J. (2002a), Theory and application of the Day plot (M_{rs}/M_s versus H_{cr}/H_c): 1. Theoretical curves and tests using titanomagnetite data, *J. Geophys. Res.*, *107*(B3), 2056, doi:10.1029/2001JB000486.

Dunlop, D. J. (2002b), Theory and application of the Day plot (M_{rs}/M_s versus H_{cr}/H_c): 2. Application to data for rocks, sediments, and soils, *J. Geophys. Res.*, *107*(B3), 2057, doi:10.1029/2001JB000487.

Dunlop, D. J., and G. West (1969), An experimental evaluation of single domain theories, *Rev. Geophys.*, *95*, 4561–4577.

Fabian, K. (2003), Some additional parameters to estimate domain state from isothermal remanent magnetization, *Earth Planet. Sci. Lett.*, *213*, 337–345.

Fabian, K., K. Andreas, W. Williams, F. Heider, T. Leibl, and A. Huber (1996), Three-dimensional micromagnetic calculations for magnetite using FFT, *Geophys. J. Int.*, *124*, 89–104.

Fukuma, K., and D. J. Dunlop (1997), Monte Carlo simulation of two-dimensional domain structures in magnetite, *J. Geophys. Res.*, *102*, 5135–5143.

Fukuma, K., and D. J. Dunlop (1998), Grain-size dependence of two-dimensional micromagnetic structures for pseudo-single-domain magnetite (0.2–2.5 μm), *Geophys. J. Int.*, *134*, 843–848.

Gee, J. S., and D. V. Kent (1997), Magnetization of axial lavas from the southern East Pacific Rise (14°–23°S): Geochemical controls on magnetic properties, *J. Geophys. Res.*, *102*, 24,873–24,886.

Gee, J. S., and D. V. Kent (1999), Calibration of magnetic granulometric trend in oceanic basalts, *Earth Planet. Sci. Lett.*, *170*, 377–390.

Geiss, C. E., F. Heider, and H. C. Soffel (1996), Magnetic domain observations on magnetite and titanomagnetite grains (0.5–10 μm), *Geophys. J. Int.*, *124*, 75–88.

Halgedahl, S. L., and M. Fuller (1983), The dependence of magnetic domain structure upon magnetization state with emphasis on nucleation as a mechanism for pseudo-single-domain behavior, *J. Geophys. Res.*, *88*, 6505–6522.

Mayergoyz, I. D. (1986), Mathematical models of hysteresis, *IEEE Trans. Magn.*, *22*(5), 603–608.

Metlov, K. L. (2000), Representability of the domain wall motion in random potentials by the Preisach model, *Phys. B*, *275*, 164–167.

Muxworthy, A., and W. Williams (1999a), Micromagnetic models of pseudo-single-domain grains of magnetite near the Verwey transition, *J. Geophys. Res.*, *104*, 29,203–29,217.

Muxworthy, A., and W. Williams (1999b), Micromagnetic calculation of hysteresis as a function of temperature in pseudo-single-domain magnetite, *Geophys. Res. Lett.*, *26*, 1065–1068.

Muxworthy, A. R., D. J. Dunlop, and W. Williams (2003a), High-temperature magnetic stability of small magnetite particles, *J. Geophys. Res.*, *108*(B5), 2281, doi:10.1029/2002JB002195.

Muxworthy, A., W. Williams, and D. Virdee (2003b), Effect of magnetostatic interactions on the hysteresis parameters of single-domain and pseudo-single-domain grains, *J. Geophys. Res.*, *108*(B11), 2517, doi:10.1029/2003JB002588.

Néel, L. (1954), Remarques sur la théorie des propiétés magnétiques des substances dures, *Appl. Sci. Res.*, *B4*, 13–24.
Newell, A., and R. Merrill (2000a), Nucleation and stability of ferromagnetic states, *J. Geophys. Res.*, *105*, 19,377–19,391.
Newell, A., and R. Merrill (2000b), Size dependence of hysteresis properties of small pseudo-single-domain grains, *J. Geophys. Res.*, *105*, 19,393–19,403.
Özdemir, O., and D. J. Dunlop (1997), Effect of crystal defects on the domain structure of magnetite, *J. Geophys. Res.*, *102*, 20,211–20,224.
Pike, C. R., A. P. Roberts, and K. L. Verosub (1999), Characterizing interactions in fine magnetic particle system using first order reversal curve, *J. Appl. Phys.*, *85*, 6660–6667.
Preisach, F. (1935), Uber die magnetische nachwirkung, *Z. Phys.*, *94*, 277–302.
Rave, W., and K. Ramstock (1997), Micromagnetic calculation of the grain size dependence of remanence and coercivity in nanocrystalline permanent magnets, *J. Magn. Magn. Mater.*, *171*, 69–82.
Rave, W., K. Fabian, and A. Hubert (1998), Magnetic states of small cubic particles with uniaxial anisotropy, *J. Magn. Magn. Mater.*, *190*, 332–348.
Roberts, A. P., C. R. Pike, and K. L. Verosub (2000), First-order reversal curve diagrams: A new tool for characterizing the magnetic properties of natural samples, *J. Geophys. Res.*, *105*, 28,461–28,475.
Schabes, M. E. (1991), Micromagnetic theory of non-uniform magnetization processes in magnetic recording particles, *J. Magn. Magn. Mater.*, *95*, 249–288.
Schabes, M. E., and H. N. Bertram (1988), Magnetization processes in ferromagnetic cubes, *J. Appl. Phys.*, *64*, 1347–1357.
Seberino, C., and H. N. Bertram (2001), Concise, efficient three-dimensional fast multipole method for micromagnetics, *IEEE Trans. Magn.*, *37*, 1078–1086.
Song, T., and R. M. Roshko (2000), Preisach model for systems of interacting superparamagnetic particles, *IEEE Trans. Magn.*, *36*, 223–230.
Song, T., R. M. Roshko, and E. D. Dahlberg (2001), Modelling the irrevirsible response of magnetically ordered materials: A Preisach-based approach, *J. Phys. Condens. Matter*, *13*, 3443–3446.
Stoner, E. C., and W. Wohlfarth (1948), A mechanism of magnetic hysteresis in heterogeneous alloys, *Philos. Trans R. Soc. London, Ser. A*, *240*, 599–642.
Tauxe, L., T. A. T. Mullender, and T. Pick (1996), Potbellies, wasp-waists, and superparamagnetism in magnetic hysteresis, *J. Geophys. Res.*, *101*, 571–583.
Tauxe, L., H. N. Bertram, and C. Seberino (2002), Physical interpretation of hysteresis loops: Micromagnetic modeling of fine particle magnetite, *Geochem. Geophys. Geosyst.*, *3*(10), 1055, doi:10.1029/2001GC000241.
Wang, D., and R. Van der Voo (2004), The hysteresis properties of multidomain magnetite and titanomagnetite/titanomaghemite in mid-ocean ridge basalts, *Earth Planet. Sci. Lett.*, *220*, 175–184.
Williams, W., and D. J. Dunlop (1989), Three-dimensional micromagnetic modeling of ferromagnetic domain structure, *Nature*, *337*, 634–637.
Williams, W., and D. J. Dunlop (1990), Some effects of grain shape and varying external magnetic field on the magnetic structure of small grains of magnetite, *Phys. Earth Planet. Inter.*, *65*, 1–14.
Williams, W., and D. J. Dunlop (1995), Simulation of magnetic hysteresis in pseudo-single-domain grains of magnetite, *J. Geophys. Res.*, *100*, 3859–3871.
Williams, W., and T. Wright (1998), High-resolution micromagnetic models of fine grains of magnetite, *J. Geophys. Res.*, *103*, 30,537–30,550.
Winklhofer, M., K. Fabian, and F. Heider (1997), Magnetic blocking temperatures of magnetite calculated with a three-dimensional micromagnetic model, *J. Geophys. Res.*, *102*, 22,695–22,709.
Xu, W., R. Van der Voo, D. R. Peacor, and R. T. Beaubouef (1997), Alteration and dissolution of fine-grained magnetite and its effects on magnetization of the ocean floor, *Earth Planet. Sci. Lett.*, *151*, 279–288.
Yu, Y. (1998), Rock magnetic and paleomagnetic experiments on hemoilmenites and titanomagnetites in some volcanic rocks from Japan, M.Sc., Univ. of Toronto, Toronto, Canada.
Yu, Y., and D. J. Dunlop (2001), Paleointensity determination on the late Precambrian Tudor Gabbro, Ontario, *J. Geophys. Res.*, *106*, 26,331–26,344.
Yu, Y., D. J. Dunlop, and Ö. Özdemir (2002), Partial anhysteretic remanent magnetization in magnetite: 1. Additivity, *J. Geophys. Res.*, *107*(B10), 2244, doi:10.1029/2001JB001249.
Yu, Y., L. Tauxe, and B. M. Moskowitz (2004), Temperature dependence of magnetic hysteresis, *Geochem. Geophys. Geosyst.*, *5*, Q06H11, doi:10.1029/2003GC000685.